

Influence of Giant CCN on warm rain processes in the ECHAM5 GCM

R. Posselt and U. Lohmann

Institute for Atmospheric and Climate Science, ETH Zurich, Universitaetsstrasse 16, 8092 Zurich, Switzerland

Received: 25 September 2007 – Published in Atmos. Chem. Phys. Discuss.: 16 October 2007

Revised: 20 June 2008 – Accepted: 20 June 2008 – Published: 17 July 2008

Abstract. Increased Cloud Condensation Nuclei (CCN) load due to anthropogenic activity might lead to non-precipitating clouds because the cloud drops become smaller (for a constant liquid water content) and, therefore, less efficient in rain formation (aerosol indirect effect). Adding giant CCN (GCCN) into such a cloud can initiate precipitation (namely, drizzle) and, therefore, might counteract the aerosol indirect effect.

The effect of GCCN on global climate on warm clouds and precipitation within the ECHAM5 General Circulation Model (GCM) is investigated. Therefore, the newly introduced prognostic rain scheme (Posselt and Lohmann, 2007) is applied so that GCCN are directly activated into rain drops. The ECHAM5 simulations with incorporated GCCN show that precipitation is affected only locally. On the global scale, the precipitation amount does not change. Cloud properties like total water (liquid + rain water) and cloud drop number show a larger sensitivity to GCCN. Depending on the amount of added GCCN, the reduction of total water and cloud drops account for up to 20% compared to the control run without GCCN. Thus, the incorporation of the GCCN accelerate the hydrological cycle so that clouds precipitate faster (but not more) and less condensed water is accumulated in the atmosphere.

An estimate of the anthropogenic aerosol indirect effect on the climate is obtained by comparing simulations for present-day and pre-industrial climate. The introduction of the prognostic rain scheme lowered the anthropogenic aerosol indirect effect significantly compared to the standard ECHAM5 with the diagnostic rain scheme. The incorporation of the GCCN changes the model state, especially the cloud properties like TWP and N_l . The precipitation changes only locally but globally the precipitation is unaffected because it has to

equal the global mean evaporation rate. Changing the cloud properties leads to a local reduction of the aerosol indirect effect and, hence, partly compensating for the increased anthropogenic CCN concentrations in that regions. Globally, the aerosol indirect effect is nearly the same for all simulations.

1 Introduction

Clouds play an important role in the energy budget of the earth. Anthropogenic influences change the radiative properties of clouds. Aerosol particles and their precursors emitted from the earth's surface, in particular, are thought to change the physical and optical properties of clouds. The first aerosol indirect effect (AIE) refers to decreasing cloud droplet sizes as the concentration of (anthropogenic) aerosols increases. For a constant liquid water content, the higher number of smaller cloud droplets leads to an increase in the cloud albedo and therefore, in the planetary albedo (Twomey, 1974; Denman et al., 2007). Furthermore, it is more unlikely that the cloud droplets will grow to precipitation sized drops. This presumably results in a prolonged lifetime of clouds within the atmosphere (Albrecht, 1989; Denman et al., 2007). This second AIE also causes an increase in the planetary albedo. However, the magnitude of both of these effects is still very uncertain.

Various studies suggested (e.g., Rosenfeld et al., 2002; Johnson, 1982; Feingold et al., 1999; Zhang et al., 2006) that the addition of giant CCN (GCCN, e.g., sea salt) possibly counteract the precipitation suppression caused by an increase in anthropogenic aerosols acting as Cloud Condensation Nuclei (CCN) and, thus, is one process that contribute to the uncertainties in the AIE. Although only very few in number, large drops resulting from the activation of GCCN enhance the collection process which leads to initiation of precipitation in an otherwise non-precipitating cloud.



Correspondence to: R. Posselt
(rebekka.posselt@env.ethz.ch)

Table 1. Sea salt production mechanisms according to Andreas et al. (1995) as function of the 10 m wind speed u_{10} .

u_{10} m s ⁻¹	mechanism	droplet type	radius μm	number cm ⁻³
>3–5	bubble breaking of the white caps of the ocean	film droplets jet droplets	<3 3–20	few hundreds few (1 to 6)
>7–11	mechanical tearing of the wave crest	spume/splash drops	>20	depending on u_{10} (O'Dowd et al., 1997)

Source regions of sea salt are the oceans (Schulz et al., 2004) whereas continental giant aerosols consist mainly of dust (Tegen et al., 2002). Sea salt is a very good CCN due to its soluble nature. In contrast, dust is insoluble and thus acts as very efficient ice nuclei (Lohmann and Diehl, 2006; Levin et al., 2005). The focus of this study is on warm clouds and precipitation only. Thus, sea salt is the more important GCCN. The influence of giant dust as IN for precipitation formation in mixed-phase clouds is neglected in the presented study.

1.1 Sea salt measurements and parameterizations

Sea salt is the dominant aerosol species (concerning mass) in the marine boundary layer (Schulz et al., 2004; Lewis and Schwartz, 2004; Denman et al., 2007). The direct effect of sea salt on climate is a cooling due to the scattering of incoming solar radiation of -1.51 to -5.03 W m⁻² at top of the atmosphere (TOA) (Schulz et al., 2004). Sea salt acts as a very good CCN and, therefore, also has an indirect effect on climate via cloud formation. The emission of sea salt is mainly driven by wind speed. Turbulent and convective mixing and gravitational settling contribute to the sea salt distribution in the marine boundary layer as well (Fitzgerald, 1991). Sea salt aerosols of different sizes form by various mechanisms (Andreas et al., 1995) which are summarized in Table 1 depending on the 10 m wind speed u_{10} .

Measurements of sea salt are usually taken in the surface layer at a height of about 10–20 m. Some observations also include towers at the shore (40 m, O'Dowd et al., 1997) and flights (Reid et al., 2001). The total particle concentration over the ocean is 100–300 cm⁻³ (Fitzgerald, 1991). Thereby, the smaller particles ($r < 3$ μm) make up 90–95 % of the total number concentration and about 5 % of total mass. These particles consist mainly of non-sea-salt sulphate. The larger the particles become the higher is the sea salt fraction, i.e., the ratio of sea salt to total aerosol. Particles larger than 0.5 μm (coarse mode aerosol) consist mainly of sea salt (~ 60 –100 %) (Lewis and Schwartz, 2004; Fitzgerald, 1991). If dust is present, then sea salt and dust are equally distributed (Fitzgerald, 1991). Coarse mode particles are found at concentrations of 5–30 cm⁻³ (Fitzgerald, 1991). Giant sea salt ($r > 5$ μm) is much less abundant. Concentrations of 10^{-4} – 10^{-2} cm⁻³ were found by Feingold et al. (1999). Smith et al. (1989) reports values of

10^{-4} – 10^{-2} cm⁻³ for calm conditions and up to 0.1–1 cm⁻³ for strong winds ($u_{10} \sim 30$ m s⁻¹).

Sea salt aerosols smaller than 10–25 μm are assumed to be well mixed in the marine boundary layer because they experience a rapid mixing and little influence of the gravity (Lewis and Schwartz, 2004; Reid et al., 2001). Particles larger than 25 μm are well mixed throughout the surface layer (few meters above the sea surface) (Lewis and Schwartz, 2004) but they are highly affected by gravitational settling. In an unstable boundary layer the mixing is enhanced by turbulence and convection, whereas in a stable atmosphere mixing and, thus, sea salt concentrations are diminished above the surface layer.

The incorporation of sea salt emissions in General Circulation Models (GCM), such as the ECHAM5, is done by a sea salt generation or source function. Usually, it is a wind dependent flux (per size) of sea salt from the ocean surface (Schulz et al., 2004). Some source functions assume steady state conditions where the surface production balances the removal by dry deposition. However, this assumption is only true for relatively small sea salt particles. The larger the particles and/or the higher the wind speeds become the longer it takes them to reach steady state (Reid et al., 2001). The derivation of the sea salt generation functions is based on field observations (e.g., Woodcock, 1953; Smith and Harrison, 1998) and (additional) laboratory measurements (e.g., Monahan et al., 1986). A limitation for these relationships is the size range covered by the instruments. Combinations of existing generation functions are used to obtain sea salt generation functions that cover larger size ranges, a variety of wind speed conditions and fit available observations (Guelle et al., 2001; Andreas, 1998).

1.2 Clouds, precipitation and Giant CCN

The impact of GCCN on the formation of precipitation is the subject of various studies. Johnson (1982) combined a condensation model with two collection models (parcel and trajectory model). Cloud water was formed on an aerosol distribution (including ultra-giant CCN: $r > 10$ μm) by condensation. Giant and ultra-giant CCN produce a tail of large droplets within the cloud droplet distribution. The resulting cloud droplets take part in collision/coalescence processes. Very large drops (~ 60 –100 μm) contribute most to the precipitation formation because they have a high collection

efficiency. It was also found that continental clouds are inefficient in producing precipitation if no giant or ultra-giant CCN are available, whereas, maritime clouds depend less on GCCN for precipitation formation. Sedimentation of droplets is considered in the trajectory model. Thus, very large drops become less important because they fall out of the cloud before taking part in the collection processes. Therefore, the drop sizes important for rain production are shifted to lower sizes ($\sim 20\text{--}50\ \mu\text{m}$) but they are still due to GCCN.

Similar studies with a wide range of models – a collection box model, a trajectory model, a 2 dimensional eddy-resolving model and a 3 dimensional large eddy simulation (LES) model – were conducted by Feingold et al. (1999). Measured GCCN concentrations of $10^{-4}\text{--}10^{-2}\ \text{cm}^{-3}$ (within the lowermost 30 m) and background aerosol concentrations of $50\text{--}250\ \text{cm}^{-3}$ were used in the model simulations. It was again found that the more GCCN were present the more drizzle was produced. Furthermore, the relative effect of the GCCN is increased with increasing background aerosol concentration (i.e., with increasing pollution). Nevertheless, the polluted cloud (high CCN concentrations) did not produce the same amount of drizzle as the clean cloud (low CCN concentration). Furthermore, it was found that a cloud in the presence of GCCN has a lower optical thickness and, therefore, a lower albedo. Hence, the GCCN might be able to moderate the effects of anthropogenic CCN on clouds and climate.

Partly contradictory results to previous studies were presented by Zhang et al. (2006). They investigated the effect of CCN concentration on precipitation in low level, warm stratiform marine and continental clouds with a one dimensional model including size-resolved cloud microphysics. They conducted two sets of numerical experiments. First they found that seeding a polluted, non-precipitating (“continental”) cloud with GCCN initiates precipitation. The GCCN lower the supersaturation in the cloud as they are preferentially activated. Small aerosol particles, originating from small droplets that evaporated in a subsaturated downdraft, do not become reactivated when they got back into a supersaturated updraft. Thus, the total number of droplets decreases, whereas the size increases which results in an enhanced rain production. Secondly they found that if GCCN are already present during cloud formation, precipitation formation is decelerated and the GCCN have only little impact on the precipitation intensity. They concluded that the activated aerosol particles cannot grow to larger sizes by condensation as the GCCN take up high amounts of the available water vapor and lower the supersaturation. This suppressed condensational growth inhibits the broadening of the drop spectra which is auxiliary in initiating rain by enhancing the collection process (see also Beheng and Doms, 1986).

Rosenfeld et al. (2002) investigated the effect of GCCN on clouds by evaluating satellite measurements. This study concentrates on deep convective clouds in the outflow region of the Indian subcontinent. The clouds disappeared the longer

they were over the ocean and the further they were away from the continent. Sea salt aerosols from the ocean get mixed into the cloud which forms relatively large drops that collect the smaller drops more efficiently and the cloud starts to precipitate. The wet deposition of aerosols by rain leads to a cleaner environment which causes subsequently formed clouds to precipitate more readily. This positive feedback results in further cleansing of the atmosphere.

Further ways of studying the effect of GCCN on clouds and precipitation formation is the seeding of clouds with hygroscopic particles (Cooper et al., 1997; Ghate et al., 2007). Burning airborne hygroscopic flares produce hygroscopic aerosol distributions that cover a size range of $0.1\ \mu\text{m}$ up to $100\ \mu\text{m}$ (Cooper et al., 1997). Both studies showed that observed size distributions of cloud droplets in seeded clouds experience a distinct broadening in comparison to the non-seeded case. This results in a higher number of larger cloud droplets ($>15\ \mu\text{m}$) which enhance the collection process and thus precipitation formation. Furthermore, the cloud droplet number concentration is decreasing resulting from a preferred activation of the larger particles which reduces the supersaturation. Thus, smaller particles do not get activated and the total number concentration is reduced.

All these studies show that the GCCN might have a non-negligible effect on the cloud and precipitation formation over the ocean. Decreasing drop number with a concurrent increase in drop size will lower the cloud albedo and, thus, result in a reduction of the cloud albedo effect. The acceleration in precipitation initiation would additionally lead to a reduction of the cloud lifetime effect. However, the effect of GCCN is not yet incorporated in GCMs suggesting that estimates of the aerosol indirect effect might be too high.

In this paper, ECHAM5 simulations are used to determine the effect of giant sea salt aerosol on cloud processes and, therefore, on precipitation formation as well as on the global radiative budget. The following section gives an overview over the ECHAM5 GCM including statements about all relevant parameterizations and the used model setup. Section 3.1 present results of a sensitivity study conducted with the ECHAM5 Single Column Model (SCM) using prescribed CCN and GCCN concentrations. In Sect. 3.2, global simulations of present-day climate are compared to pre-industrial simulations both with and without incorporated GCCN. The conclusions of this study are summarized in Sect. 4.

2 Model description and setup

2.1 The general circulation model ECHAM5

The ECHAM5-GCM is based on the ECMWF model and has been further developed at the Max-Planck-Institute for Meteorology in Hamburg. Within ECHAM5 the prognostic equations for temperature, surface pressure, divergence and vorticity are solved on a spectral grid with a triangular truncation

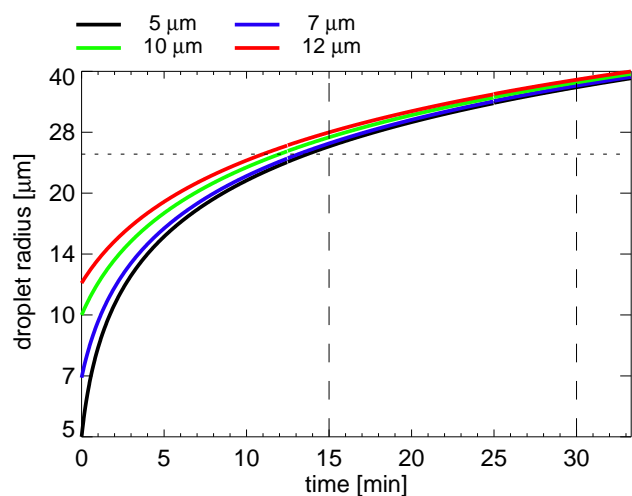


Fig. 1. Condensational growth of different sized GCCN particles.

(Roeckner et al., 2003). Prognostic equations for cloud water and cloud drop number concentration, for cloud ice and the ice crystal number concentration as well as detailed cloud microphysics are used according to Lohmann et al. (2007). In order to incorporate the GCCN and their effect on precipitation properly, prognostic equations for rain water mass mixing ratio and rain drop number concentration were introduced into the ECHAM5 (Posselt and Lohmann, 2007). Considered processes include autoconversion of cloud droplets to rain and accretion of cloud droplets by rain (Khairoutdinov and Kogan, 2000), self-collection of rain drops (Seifert and Beheng, 2001), evaporation of rain (Rotstajn, 1997) and melting of snow (Lohmann and Roeckner, 1996). The sedimentation of the rain drops is treated as a vertical one dimensional advection with an explicit fall speed for mass and number, respectively. The fall speed is a function of rain water mass and number and is limited by the grid velocity (layer height/model time step). Furthermore, all processes involved in rain formation are evaluated repeatedly on smaller sub-time steps within one model time step. Single Column Model (SCM) simulations by Posselt and Lohmann (2007) showed that the prognostic rain scheme has little influence on the precipitation amount itself but it shifts the emphasis from autoconversion to accretion in better agreement with observations (Wood, 2005). Convection within ECHAM5 is parameterized according to Tiedtke (1989) with modifications presented by Nordeng (1994). Within this scheme convection is triggered by the large-scale moisture convergence. Its magnitude also determines whether the deep convection or shallow convection scheme is used. Convective precipitation is only formed in the deep convection scheme where it is assumed to be proportional to the liquid water content. Thus, aerosol number and composition do not influence convective precipitation formation.

2.2 Coupling GCCN and Prognostic Rain

Atmospheric aerosol distributions are represented by a double moment scheme consisting of a superposition of 7 log-normal distributions of different size ranges, solubilities, and chemical constituents within the aerosol module HAM (Stier et al., 2005). GCCN are not explicitly included in the HAM thus soluble coarse mode particles with $r > 10 \mu\text{m}$ (GCCN₁₀) or $r > 5 \mu\text{m}$ (GCCN₅) are regarded as GCCN in this study. It is further assumed that over the ocean the coarse mode aerosol consists only of sea salt. The GCCN get activated together with the rest of the aerosol particles by the activation scheme of Lin and Leitch (1997). This is an empirical scheme that only depends on aerosol number and vertical velocity. Thus, the competition effect of GCCN and CCN and the lowering of the supersaturation by the GCCN is not included. The activation of the aerosol particles and the following condensation of water vapor onto the particles assuming saturation adjustment (Roeckner et al., 2003) is done for the whole aerosol spectra. GCCN are not treated separately. Afterwards, the total condensed liquid water is redistributed between the rain water mixing ratio which corresponds to the water uptake by the GCCN and the cloud water mixing ratio which is due to the activation of the CCN. The redistribution is based on the number of activated GCCN. The number of rain drops formed by the activation of GCCN is equal to the number of activated GCCN. The rain water formed by the activation of GCCN is given by the mass of the newly formed rain drop times the number of activated GCCN and is limited by the total amount of condensed water. The radius of the rain drops originating from GCCN is assumed to be $25 \mu\text{m}$. This radius is chosen analogous to the rain drop distinction radius used by Khairoutdinov and Kogan (2000) in their cloud microphysics parameterization. Sensitivity studies with the ECHAM5 single column model (SCM, presented in Sect. 3.1) also showed that this choice of the rain drop radius is reasonable. Larger drop sizes would introduce problems regarding the transfer of condensed water to the rain class and smaller droplets would not belong to the rain class according to the definition of Khairoutdinov and Kogan (2000). Figure 1 gives an estimate over the condensational growth of different sized aerosol particles within the range of one model time step. It can be seen that even the smallest GCCN ($5 \mu\text{m}$) grows to more than $25 \mu\text{m}$ in less than 15 min, i.e., within less than one model time step.

The schematic in Fig. 2 summarizes the changes within the large-scale cloud microphysics scheme due to the GCCN. Thereby, changes or additions are marked in blue. This includes the retrieval of the GCCN number concentration from the HAM aerosols and their subsequent activation to rain drops with a radius of $25 \mu\text{m}$ within the prognostic rain scheme.

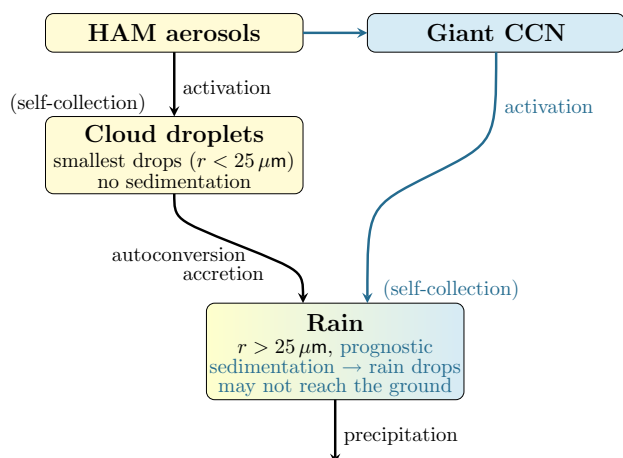


Fig. 2. Schematic of the coupling of the GCCN to the large-scale cloud microphysics scheme. Parts in blue represent changes or additions to the standard large-scale cloud microphysics scheme.

2.3 Model setup

The SCM simulations are conducted at a T63 horizontal resolution (corresponds to $1.875^\circ \times 1.875^\circ$). In the vertical, 31 model levels are used with the uppermost layer at 10 hPa. A simulation time step of 15 min is applied. Meteorological conditions are forced using data from the EPIC (Eastern Pacific Investigation of Climate Processes) campaign (Bretherton et al., 2004) which took place in September and October 2001 in the eastern Pacific off the coast of Ecuador and Peru (see also Posselt and Lohmann, 2007).

For the global simulations, a T42 horizontal resolution (corresponds to $2.8125^\circ \times 2.8125^\circ$) with 19 vertical model levels (uppermost layer at 10 hPa) and a time step of 30 min is used. The simulations are integrated for 10 years after a 3 month spin-up using climatological sea-surface temperatures and sea-ice extend. For the simulations in this study the relative humidity based cloud cover scheme of Sundqvist et al. (1989) is used. The conducted global simulations are summarized in Table 2. They include control simulations for two different numbers of sub-time steps in the prognostic rain scheme (CTL30 and CTL10) and simulations with incorporated GCCN at two different cutoff radii (GCCN₁₀ and GCCN₅) with 30 sub-time steps. The control runs are tuned so that the radiative balance at top-of-the-atmosphere (TOA) is within $\pm 1 \text{ W m}^{-2}$. The aerosol indirect effect (AIE) is estimated by comparing present-day (PD) to pre-industrial (PI) simulations. For the PI simulation, aerosol emission representative of the year 1750 are used (Dentener et al., 2006).

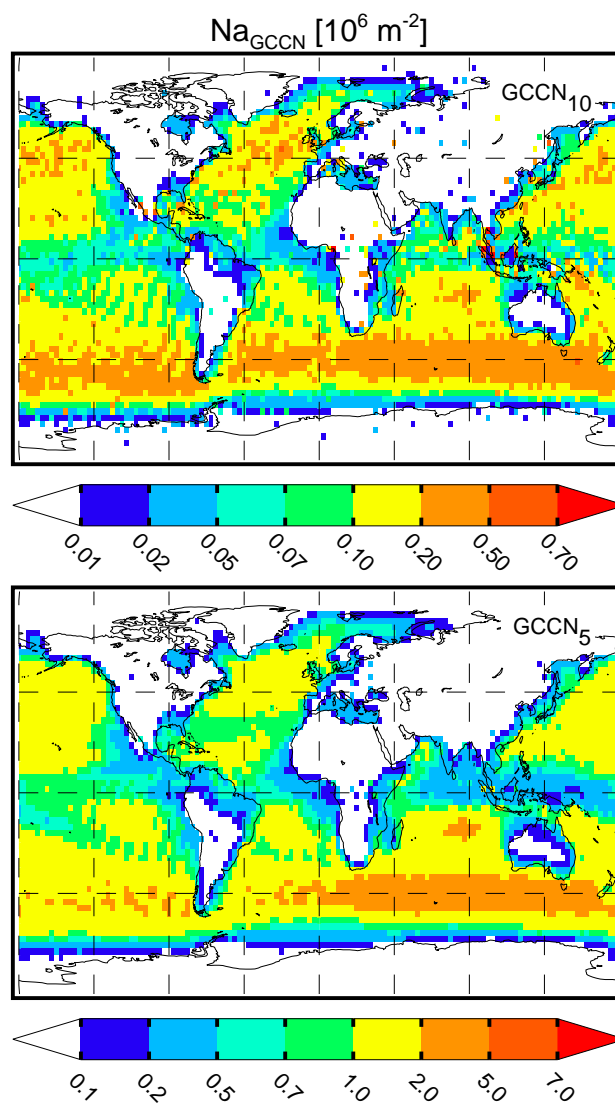


Fig. 3. Column integrated GCCN burden [10^{-6} m^{-2}] for the cutoff radii 10 μm (upper panel) and 5 μm (lower panel). Note the different scales.

2.4 Validation of modeled GCCN concentrations with observations

A realistic estimate of the effect of GCCN on clouds, precipitation and the global radiative budget is based on a realistic representation of the GCCN within the ECHAM5. This section tries to validate the modeled GCCN concentrations with observed values. Drawback of this task is the relatively sparse observational data that are only available for certain limited regions and for a very limited duration. Nevertheless, the comparison helps to assess the reliability of the simulations.

Table 2. Summary of presented global simulations.

Simulation	Description
CTL30	Control simulation; Simulation with ECHAM5-HAM (Lohmann et al., 2007) and the prognostic rain scheme by (Posselt and Lohmann, 2007) with 30 sub-time steps
CTL10	Same as CTL30 but with 10 sub-time steps in the prognostic rain scheme
GCCN ₁₀	Same as CTL30 but with included GCCN at a cutoff radius of 10 μm
GCCN ₅	Same as GCCN ₁₀ but with a cutoff radius of 5 μm

The column integrated GCCN burden obtained by GCCN₁₀ and GCCN₅ are shown in Fig. 3. The GCCN burden is about 4 to 5 orders of magnitude lower than the total aerosol burden within ECHAM5. The highest GCCN loads are present in the storm tracks of the southern ocean and the north Atlantic and Pacific where high wind speeds are predominant. Relatively low GCCN burdens are found in the tropics and off the west coasts of the continents, which results from rather low wind speeds in these areas. Over the continents, GCCN are mainly found in coastal regions close to the oceans implying that transport of marine aerosol leads to GCCN burdens over continents. Nevertheless, the GCCN burden over the continents is very low (at least 1 order of magnitude lower than over the ocean) so that the main impact of the GCCN is assumed to be over the ocean. The cutoff radius has a strong impact on the GCCN load of the atmosphere. Doubling the cutoff radius from 5 μm to 10 μm causes a decrease in GCCN burden by an order of magnitude.

Figure 4 shows sea salt number distributions for different wind speed classes from observations and from ECHAM5-HAM (Lohmann et al., 2007). The observed size distribution were taken from Lewis and Schwartz (2004). They compiled measurements from various authors, converted the distributions to number distributions ($dn/d \ln(r)$) and arranged them according to the reported wind speed. The observations were taken over the northern Atlantic, at measuring sites along the eastern and western US, during ship cruises in the East-China Sea, the Indian Ocean and within the southern storm track. The presented measurements were taken at heights of 5 to 20 m above sea level. Within the well mixed marine boundary layer the concentrations should not vary much with height. Measuring techniques include impaction sampling on filters or glass slides with subsequent investigation by electron microscopy, optical detection of aerosol particles and thermal volatility measurements. In their compilation Lewis and Schwartz (2004) excluded measurements of continental air masses (at maritime sites) and measurements from surf zones. The simulated size distributions are represented by the superposition of the soluble accumulation and coarse mode distribution of the aerosol module HAM limited to the oceans as an annual global mean. As a measure of variability of the size distribution the minimum-maximum range of the observations and the 5% and 95% percentiles of the simulation are shown as well.

It can be seen that the simulated sea salt size distribution reproduces the observations quite well. However, the simulation shows a tendency to slightly underestimate the observed size distributions. The simulated number of giant sea salt particles shows a larger underestimation especially for higher wind speeds but the concentrations within this size range are rather low. However, one has also to bear in mind that the observations are limited to certain areas and cover only some days of measurements whereas the simulations give an annual mean of all aerosol distributions over the oceans. Considering these limitations, the assumption of using the tail of the coarse mode distribution to obtain the GCCN concentration is appropriate.

Further validation of the giant sea salt concentration is done by a point-to-point comparison of observed and simulated concentrations. Therefore, the number distributions reported by Lewis and Schwartz (2004) are integrated with respect to the chosen cutoff radius of 5 or 10 μm . The obtained concentrations are then compared to the simulated GCCN concentration at the same location in the lowest model level. The results are presented in Fig. 5. First of all it can be seen that the natural variability of the GCCN concentration is much larger than the simulated one because the modeled concentrations depend mainly on the wind speed whereas the observed concentration are also influenced by various other factors. Lewis and Schwartz (2004) stated that the variability of the measured sea salt concentration is rather large even if measured at the same location and with the same instrument. They argued that the sea salt concentration depends not only on the wind speed but also on the ambient relative humidity, the stability of the atmosphere, the mixing layer height, the time since the last rain and the history of all of these factors within the measured air mass. The comparison for the 5 μm cutoff (Fig. 5, lower panel) shows that the ECHAM5 underestimates the GCCN concentrations. A large portion of the data points are more than a factor of 10 smaller than the observed values. Using a cutoff radius of 10 μm (Fig. 5, upper panel) improves the agreement between simulated and observed GCCN concentrations. Most model data fall within a factor of 10 of the observations. Furthermore, the obtained GCCN concentrations for the 10 μm cutoff agree much better with the GCCN concentrations of 10^{-2} – 10^{-4} cm^{-3} reported by Feingold et al. (1999).

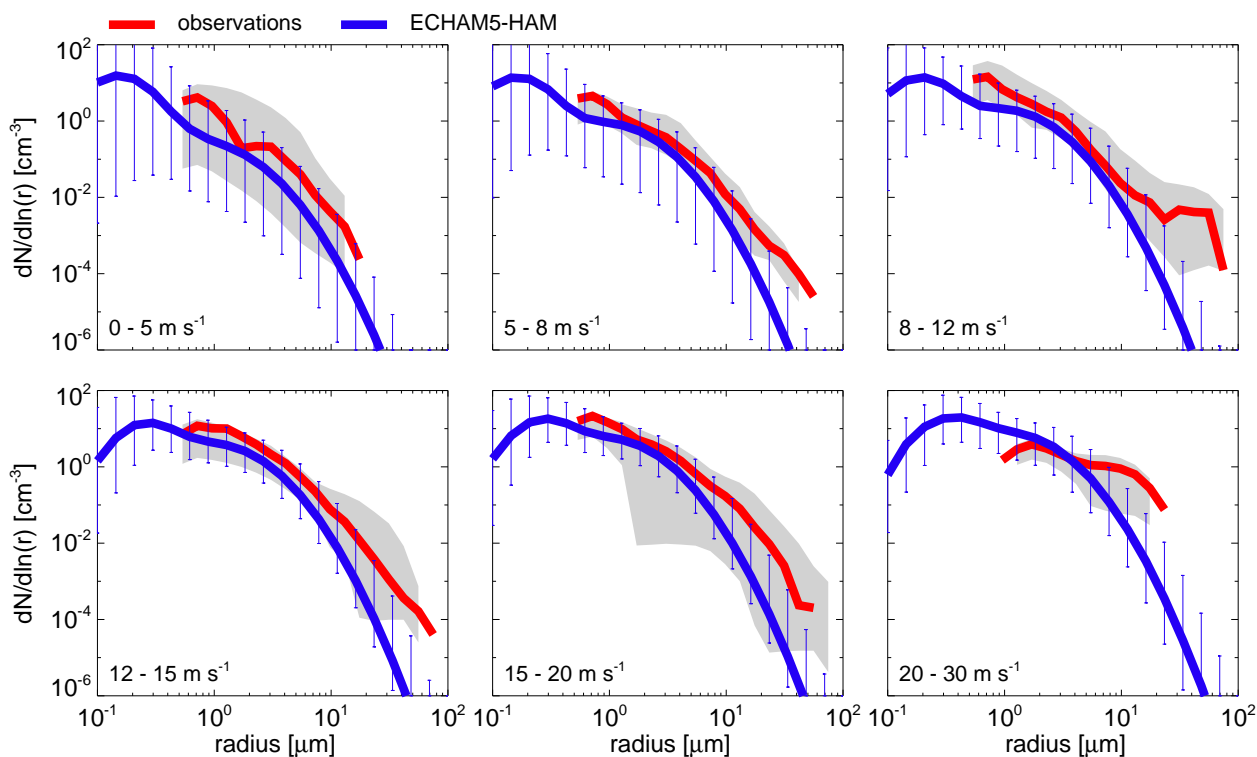


Fig. 4. Sea salt number distributions for different wind speed ranges from observations (red, median with minimum to maximum range in gray) and from simulations (blue, median with 5% and 95% percentile as error bars).

3 Results and discussion

3.1 SCM sensitivity study

This sensitivity study is carried out to evaluate the behavior of the prognostic rain scheme with the incorporated GCCN. It is conducted with the single column version of ECHAM5. The set up is similar to Feingold et al. (1999) but with different parameters. The number of GCCN is prescribed with 10^{-4} , 10^{-3} , 10^{-2} , 10^{-1} and 1 cm^{-3} . The number of background CCN is prescribed with 100, 250 and 500 cm^{-3} . For this sensitivity study, the size of the activated GCCN rain drops is varied between 12, 25 or $55 \mu\text{m}$. These values are chosen so that volume and mass of the GCCN induced rain drops experiences a tenfold increase from the smaller to the larger size. The larger the generated rain drops the more condensed water is transferred into rain water and the less water is available for the cloud droplets.

The results shown in Fig. 6 are averages over the whole simulation period of 6 days. The effect of the GCCN is only visible at quite high GCCN ($>10^{-2} \text{ cm}^{-3}$) and CCN ($\leq 250 \text{ cm}^{-3}$) concentrations. The large-scale precipitation at cloud base and at the surface (Fig. 6, upper row) decreases with increasing CCN concentrations. This is known as the second aerosol indirect effect where more but smaller cloud droplets are less efficient in rain production and in the ab-

sence of more efficient entrainment and evaporation lead to reduced precipitation and a longer cloud lifetime. An increase in GCCN results in a concurrent increase in precipitation. The incorporation of the GCCN cannot, however, completely compensate the effect of the increased CCN concentrations. In case of high GCCN concentration ($>10^{-1} \text{ cm}^{-3}$ and a large initial rain drop size ($55 \mu\text{m}$) the precipitation increase is decelerated or even reversed. This is due to the large fraction of condensed liquid water that is transferred to rain water by the activation of GCCN so that only little cloud water is left. The activation ratio (=ratio of transferred rain water due to activation of GCCN to total condensed water) is shown in Fig. 6 (middle left panel). It can be seen that the larger the assumed rain drop size or the larger the GCCN concentration the closer the transfer ratio approaches one (which means all condensed water is transferred into the rain class). In these cases the lack of cloud water inhibits autoconversion and accretion so that rain drops cannot grow and no additional rain formation takes place. Note, that a transfer ratio of one is purely artificial due to the chosen distribution mechanism and cannot be found in the real atmosphere.

The effect of the GCCN on the surface precipitation is less pronounced than for the precipitation at cloud base. The regulating process is the evaporation of rain below the cloud base. Higher precipitation amounts lead to more evaporation which removes part of the differences visible at cloud base.

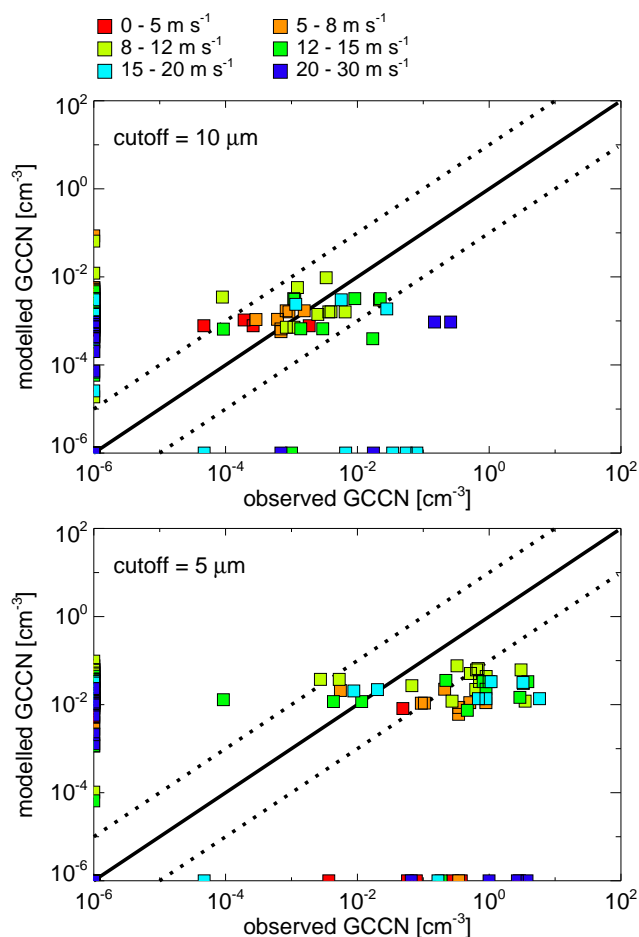


Fig. 5. Scatter plot of simulated and measured giant sea salt concentrations [cm^{-3}] for a cutoff radius of $10\ \mu\text{m}$ (upper panel) and $5\ \mu\text{m}$ (lower panel) for different wind speed ranges.

The total water path is the sum of liquid water path and the rain water path ($\text{TWP}=\text{LWP}+\text{RWP}$). The TWP is larger for a higher number of CCN but is decreasing as the number of GCCN is increasing (see Fig. 6, middle right panel). This corresponds to changes in precipitation. The changes in TWP are mainly due to changes in LWP. The more GCCN are used and the larger the initial rain drop size the larger is the initial RWP and, therefore, the LWP is decreasing. This causes the described reduction of the autoconversion and accretion rates. The equilibrium RWP is quite constant with regard to the GCCN concentrations because any additional rain water is falling out as precipitation. Similar to the precipitation, RWP is lower for higher CCN concentrations.

3.2 Global simulations

3.2.1 Model validation

The results of the global simulations with present-day emissions are summarized as annual zonal means in Fig. 7 and as annual global means in Table 3 for the CTL30, GCCN₁₀, GCCN₅ simulations and additionally for the CTL10 simulation. The results show that some of the considered variables are quite susceptible to the incorporation of the GCCN whereas others do not depend on them at all.

The incorporation of the GCCN hardly affects the precipitation amount zonally and globally. Compared to CTL30 (Table 3), the total precipitation amount is hardly affected by the incorporation of the GCCN or by the number of sub-time steps within the prognostic rain scheme (CTL30 vs. CTL10). This can also be seen in the annual zonal mean plot of Fig. 7. Compared to the monthly averaged precipitation fields from the Global Precipitation Climatology Project (GPCP) dataset (Huffman et al., 1997; Adler et al., 2003) ECHAM5 generally produces too much precipitation. The precipitation in the tropics is overestimated by ECHAM5 which points to deficiencies in the convective cloud scheme. Nevertheless, the overall agreement in the zonal distribution is satisfactory.

The annual global mean of total simulated cloud cover (Table 3) is also hardly affected by the GCCN or the number of sub-time steps. All simulations produce a cloud cover that is at the lower end of the observations of the International Satellite Cloud Climatology Project (ISCCP, Rossow and Schiffer, 1999) and from surface observations collected by Hahn et al. (1994). For the zonal mean, the agreement is best in the tropics and in the midlatitudes but in the subtropics the cloud cover is largely underestimated due to an underrepresentation of stratocumulus cloud decks off the west coasts of North and South America and Africa. In higher latitudes, differences are due to the uncertainties in the measurements. The global mean cloud cover is slightly decreasing for the GCCN simulations but the differences the zonal distributions are mainly in the southern subtropics.

The observed LWP by satellite (SSM/I) retrievals of the LWP (Greenwald et al. (1993); Weng and Grody (1994); Wentz (1997) is compared to the TWP (over the oceans) of the simulations because the model artificially distinguishes between the smaller cloud drops and the larger rain drops that the satellites do not make. The TWP produced by all simulations fall within the range given by the observations. The incorporation of the GCCN leads to a decrease in the TWP. The main decrease appears in the midlatitudes and subtropics where the precipitation formation is mainly done via the large-scale cloud scheme. The TWP within the tropics is not affected by the GCCN. The changes in TWP are caused by the changes in the LWP whereas the RWP stays nearly constant for all simulations (with the same number of sub-time steps). The decrease in LWP results from the enhanced transfer of cloud water to rain water either by the activation of the

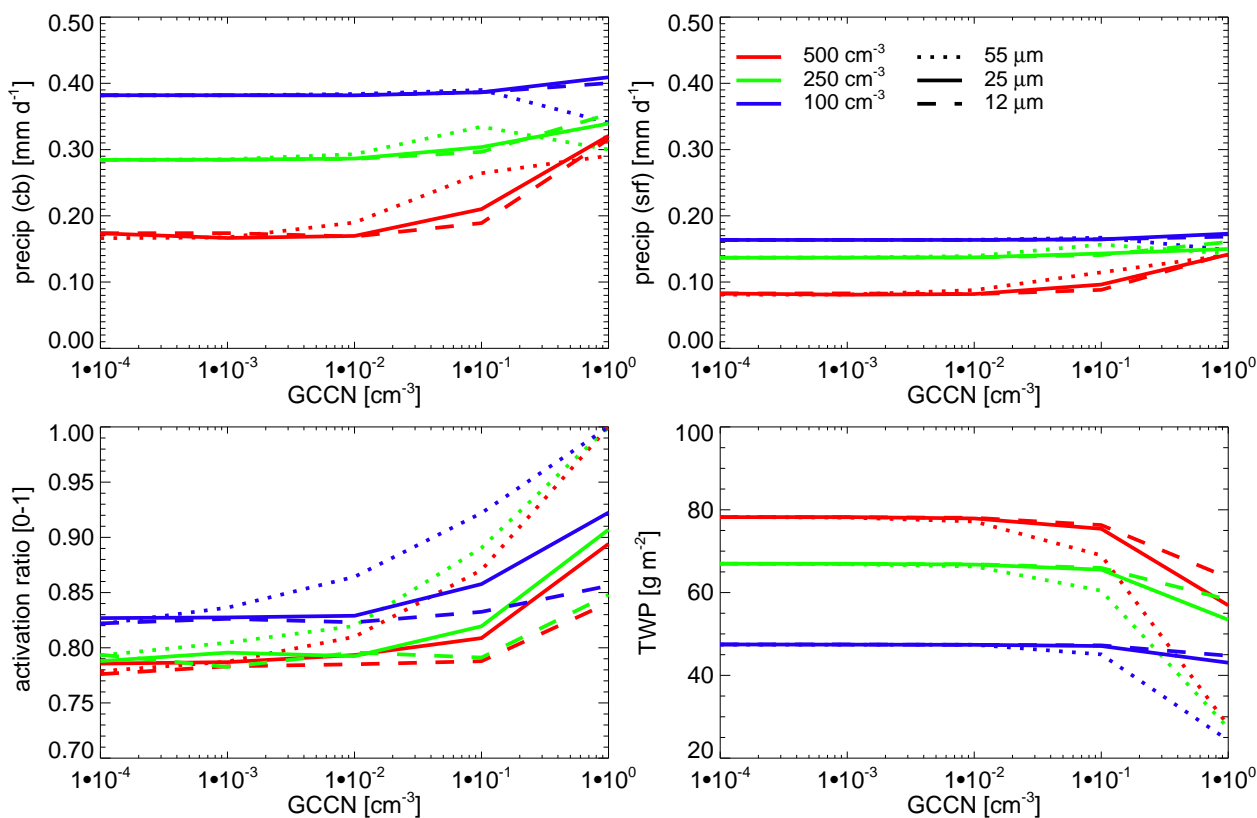


Fig. 6. SCM sensitivity study for large scale precipitation at cloud base and at the surface (upper panels), the activation ration (lower left panel) and the TWP (lower right panel) panel) with different GCCN concentrations, CCN concentrations and activated GCCN-drop radius for 30 sub-time steps.

Table 3. Annual global mean cloud properties and TOA energy budget.

		CTL30	GCCN ₁₀	GCCN ₅	CTL10	OBS
P_{tot}	[mm d ⁻¹]	2.89	2.89	2.88	2.88	2.74
P_{strat}	[mm d ⁻¹]	1.07	1.07	1.06	1.07	–
P_{conv}	[mm d ⁻¹]	1.82	1.82	1.82	1.82	–
TCC	[%]	63.3	63.2	62.7	62.8	62 – 67
TWP	[g m ⁻²]	74.6	72.9	67.7	63.3	50 – 4
LWP	[g m ⁻²]	66.7	65.0	59.6	57.3	–
RWP	[g m ⁻²]	7.9	7.9	8.1	6.0	–
N_l	[10 ¹⁰ m ⁻²]	2.2	2.1	1.9	1.9	4
R_{eff}	[μm]	11.0	11.0	11.0	10.5	11.4
SCF	[W m ⁻²]	–53.8	–53.5	–52.2	–52.0	–50
LCF	[W m ⁻²]	29.4	29.4	29.3	29.3	22 – 30

GCCN or by enhanced collection processes (e.g., accretion). The additional rain water is then removed due to sedimentation so that the RWP stays constant. However, this does not cause an increase in precipitation (as shown above) but rather an acceleration of the hydrological cycle with shorter residence times and less accumulation of water in the atmosphere.

Observations of vertically integrated cloud drop number N_l and effective radius R_{eff} at cloud top for warm clouds ($T > 0^\circ\text{C}$) are retrieved from the ISCCP dataset by Han et al. (1994, 1998) for an area between -50° and 50° based on four months of 1987. The annual global means show that the ECHAM5 simulations of N_l underestimate the observations by a factor of two. The zonal mean of N_l shows an

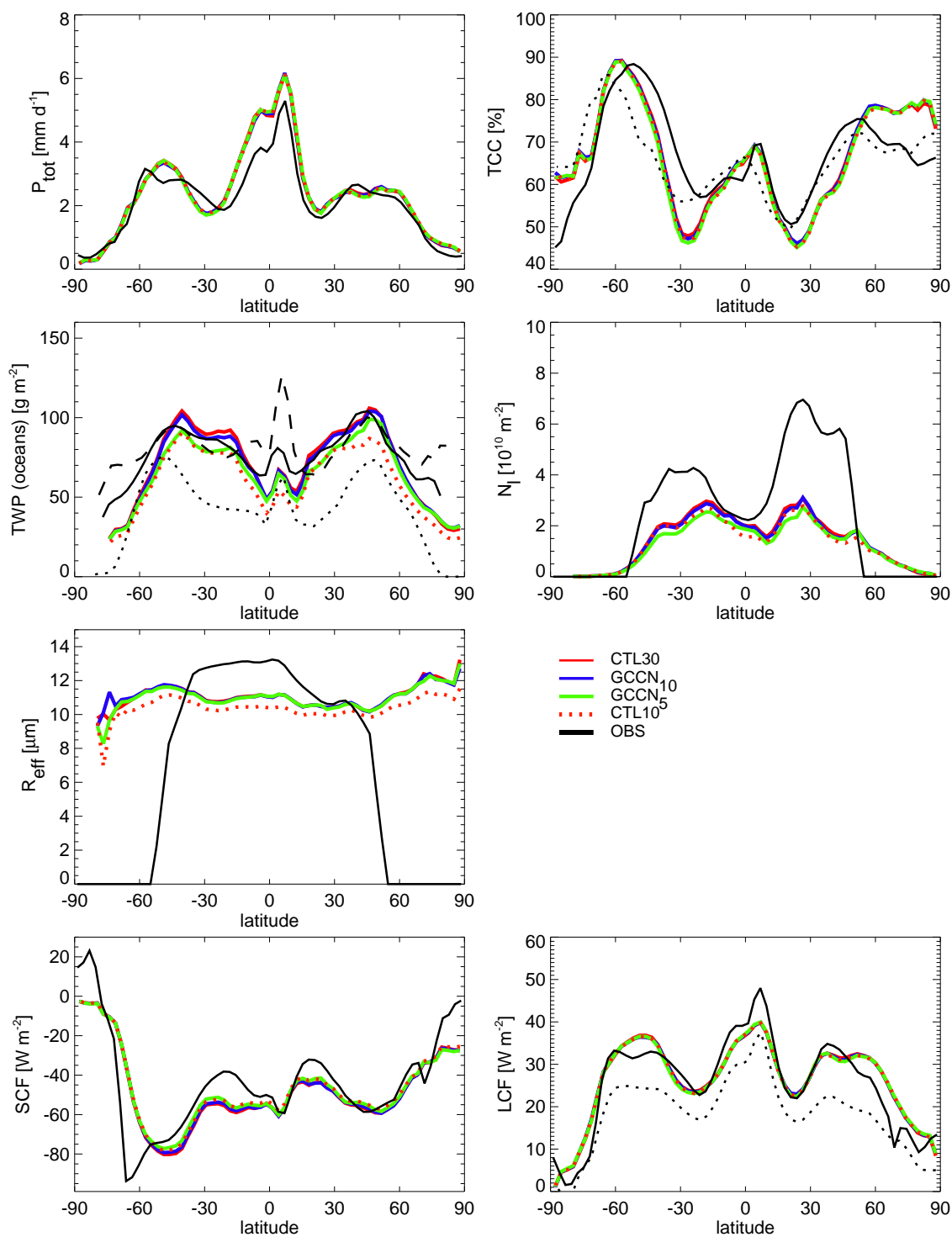


Fig. 7. Annual zonal means of precipitation, total cloud cover, total water path (only over the oceans), column integrated cloud droplet number, effective cloud droplet radius at cloud top ($T > 273.15$ K) and short-wave and long-wave cloud forcing from CTL30, GCCN₁₀, GCCN₅, and CTL10 simulations and from observations.

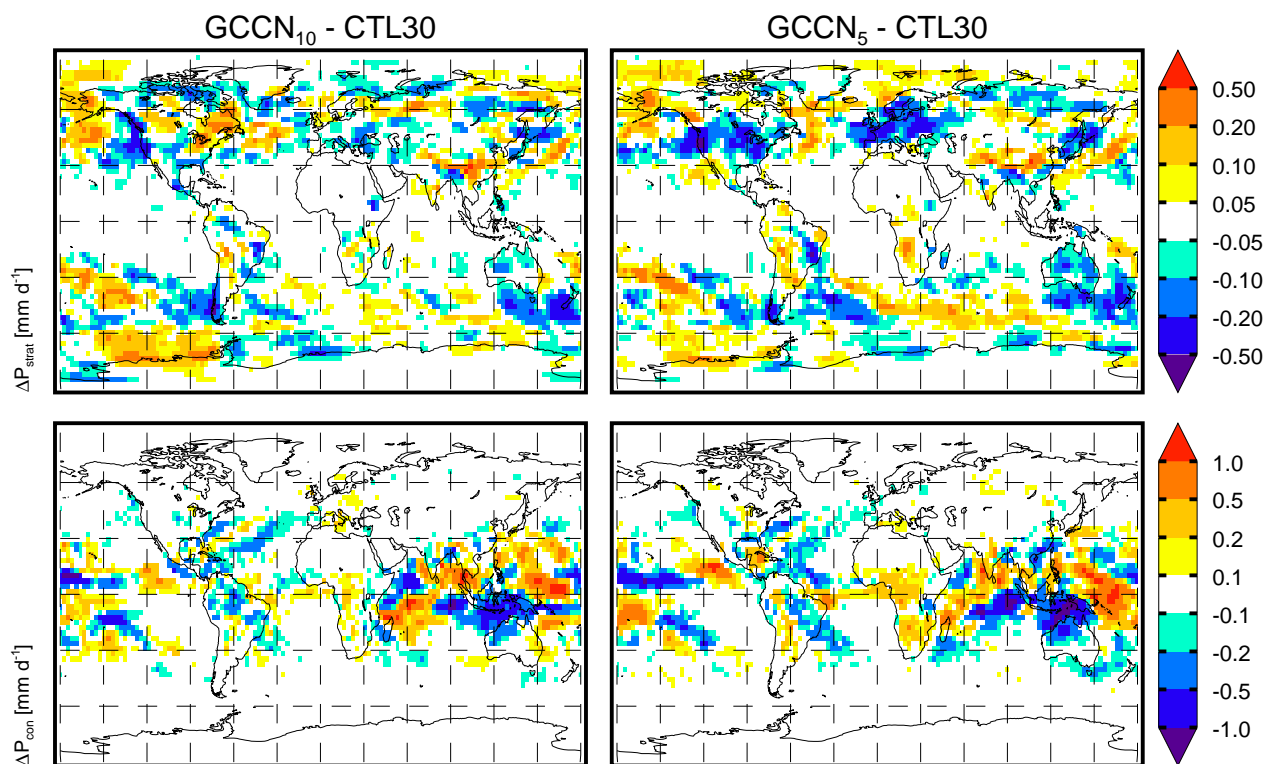


Fig. 8. Differences in the global distribution of stratiform (upper row) and convective (lower row) precipitation between the GCCN₁₀ (left column) and GCCN₅ (right column) simulations and CTL30 (please note the different scales).

underestimation in the midlatitudes especially on the northern hemisphere for all simulations. Similar to the TWP, N_1 is decreasing with higher amounts of GCCN. This results in a quite constant R_{eff} for all simulations but compared to the observations R_{eff} is underestimated.

The shown simulations also contain mixed phase and ice clouds, but there is no noticeable effect of the GCCN on the ice phase. The ice water path for the ECHAM5-PROG and ECHAM5-GCCN_{10,5} simulations are nearly the same (27.6, 27.6, 27.5 g m⁻², respectively).

Short-wave and long-wave cloud forcing (SCF and LCF) provide an estimate of the impact of clouds on the global radiative budget. The simulated SCF and LCF agree quite well with the observed values obtained from the Earth radiation budget experiment (ERBE, Kiehl et al., 1994) except in higher latitudes for the SCF and in the tropics for the LCF. For the LCF, additional data from the TOVS-B satellite (Susskind et al., 1997) is shown which give better agreement with the ECHAM5 data in the tropics but is lower in the mid-latitudes. The SCF, which is mainly affected by low clouds, become less negative with increasing amount of GCCN which means that the clouds influence the radiative budget slightly less either by their amount or by their albedo. The slight decrease in the TCC might be one reason for the change in SCF whereas cloud albedo as function of the cloud droplet size (R_{eff}) does hardly change (see above).

The LCF, representing especially high clouds, hardly show any changes and is not affected by the amount of GCCN and the number of sub-time steps within the prognostic rain scheme.

The results for CTL10 presented in Table 3 show that the set-up of the prognostic rain scheme (namely the number of sub-time steps) influences mainly the in-cloud properties like TWP (including LWP and RWP), N_1 and, consequently, R_{eff} . The TWP in CTL10 is reduced in comparison to CTL30 due to lower LWP and RWP. The reduction in LWP and N_1 is caused by higher total conversion rates (autoconversion+accretion) as it is shown in Table 4. Furthermore, the number of sub-time steps within the prognostic rain scheme are more important than the amount of GCCN in terms of the importance of the autoconversion versus the accretion rate. The lower the number of sub-time steps the higher is the importance of autoconversion on the rain formation. The ratio of autoconversion to the total conversion rate ($\text{AUT}/(\text{AUT}+\text{ACC})$) is reduced by a factor of two from 14.3% for CTL10 to 7% for CTL30. The reduction in RWP is mainly caused by a faster sedimentation of rain drops for the CTL10 simulation and thus, less rain water can accumulate within the atmosphere. Due to the reduction in RWP and LWP, the accretion rate for the CTL10-simulation is lower than for the CTL30-simulation because the accretion rate depends almost linearly on the cloud water and rain

Table 4. Annual global mean of vertically integrated autoconversion (AUT), accretion (ACC) and total conversion (AUT+ACC) rate as well as the ratio of autoconversion to total conversion rate for CTL30, GCCN₁₀, GCCN₅ and CTL10.

		CTL30	GCCN ₁₀	GCCN ₅	CTL10
AUT	kg m ⁻² s ⁻¹	0.46	0.46	0.45	0.97
ACC	kg m ⁻² s ⁻¹	6.13	6.12	6.12	5.82
AUT+ACC	kg m ⁻² s ⁻¹	6.59	6.58	6.57	6.79
AUT/(AUT+ACC)	%	7.0	7.0	6.8	14.3

water content. Another interesting feature is the similarity of CTL10 and the GCCN₅-simulation which can be seen from Table 3 and also from the annual zonal means in Fig. 7. This implies that the activation of GCCN into drizzle as additional conversion process in the GCCN₅-simulation partly compensates the loss in total conversion rate compared to CTL10.

3.2.2 Effect of GCCN on global distributions of cloud parameters and precipitation

Further insight into the impact of the GCCN on the global scale are obtained by looking into the global difference distributions of precipitation (large scale and convective), of TWP and conversion rate (autoconversion+accretion) and of PPW (precipitable water) and vertical velocity due to CAPE (convective available potential energy) which are shown in Fig. 8–10, respectively. All shown variables are vertically integrated annual means. The difference distributions are calculated between the GCCN-simulations and the control run.

Figure 8 shows the global difference distributions of stratiform and convective precipitation. Changes in the stratiform precipitation are mainly located in the midlatitudes along the storm tracks. It can be seen that regions of increased and decreased precipitation rates alternate along the zonal band so that the changes cancel each other in the zonal mean. The differences in stratiform precipitation show similar patterns for both GCCN simulations with a slightly higher magnitude for the GCCN₁₀-CTL30 case. This implies that the formation of stratiform precipitation itself depends only on whether GCCN are considered and not on the concentration and the associated transfer of condensed water to the rain class.

This is further illustrated by the global difference distribution of TWP and total conversion rate in Fig. 9. The TWP shows a strong dependence on the amount of GCCN which is closely connected to the amount of GCCN and the transfer of condensed water. The higher the GCCN concentration the higher is the transfer ratio as was shown in the SCM sensitivity study in Sect. 3.1. Thus, cloud water (i.e., the LWP) is reduced as large amounts of condensed water are transferred to rain water. The RWP stays fairly constant throughout all simulations (with the same number of sub-time steps) because all “excessive” rain water is removed from the atmosphere by sedimentation. Although TWP is reduced quite

significantly, autoconversion and accretion rate are hardly affected by the presence of GCCN (see Fig. 9, lower row and Table 4). Compared to the patterns for the stratiform precipitation it reveals a quite good correlation of 0.73 and 0.77 for GCCN₁₀-CTL30 and GCCN₅-CTL30, respectively. Processes like evaporation below cloud base that also affect the surface precipitation amount are not included in the correlation.

These results imply that the reduction in TWP due to the GCCN is not large enough to change the autoconversion and accretion rates significantly. One important process missing here is the competition effect of GCCN and CCN during activation. As GCCN would activate preferentially, less of the smaller CCN would activate which result in a lower number of cloud droplets. This in turn could cause an increase in the autoconversion rate and could lead to higher precipitation rates. But, with the current activation scheme by Lin and Leitch (1997) it is not possible to consider that process.

Convective precipitation is not directly influenced by GCCN (and aerosols, in general). Nevertheless, the incorporation of GCCN changes the amount and location of convection significantly (Fig. 8, lower row). Differences in convective precipitation between the GCCN simulations and the control run have a higher magnitude than those for the stratiform precipitation. In both considered cases the magnitude of the difference is similar but the patterns differ substantially. As there is no direct influence of the GCCN the changes must be caused by feedbacks of the convection scheme to the changes in the hydrological state of the model.

Figure 10 shows PPW (precipitable water=vertically integrated water vapor) and the vertical velocity generated by CAPE. It can be seen that the PPW distribution is altered significantly by incorporation of the GCCN and subsequent changes in the stratiform cloud scheme. The changes include variations in the evaporation rate of rain below cloud base due to changed precipitation amounts as well as variations in the evaporation of cloud droplets in cloud free air due to the changes in the cloud water content. Comparing the changes in PPW (in the tropics) and in convective precipitation similar patterns are visible. The correlation coefficient (limited to tropical regions, 30° S to 30° N) is 0.53 and 0.51 for GCCN₁₀-CTL30 and GCCN₅-CTL30, respectively. Changes in the moisture field lead inevitably to changes in

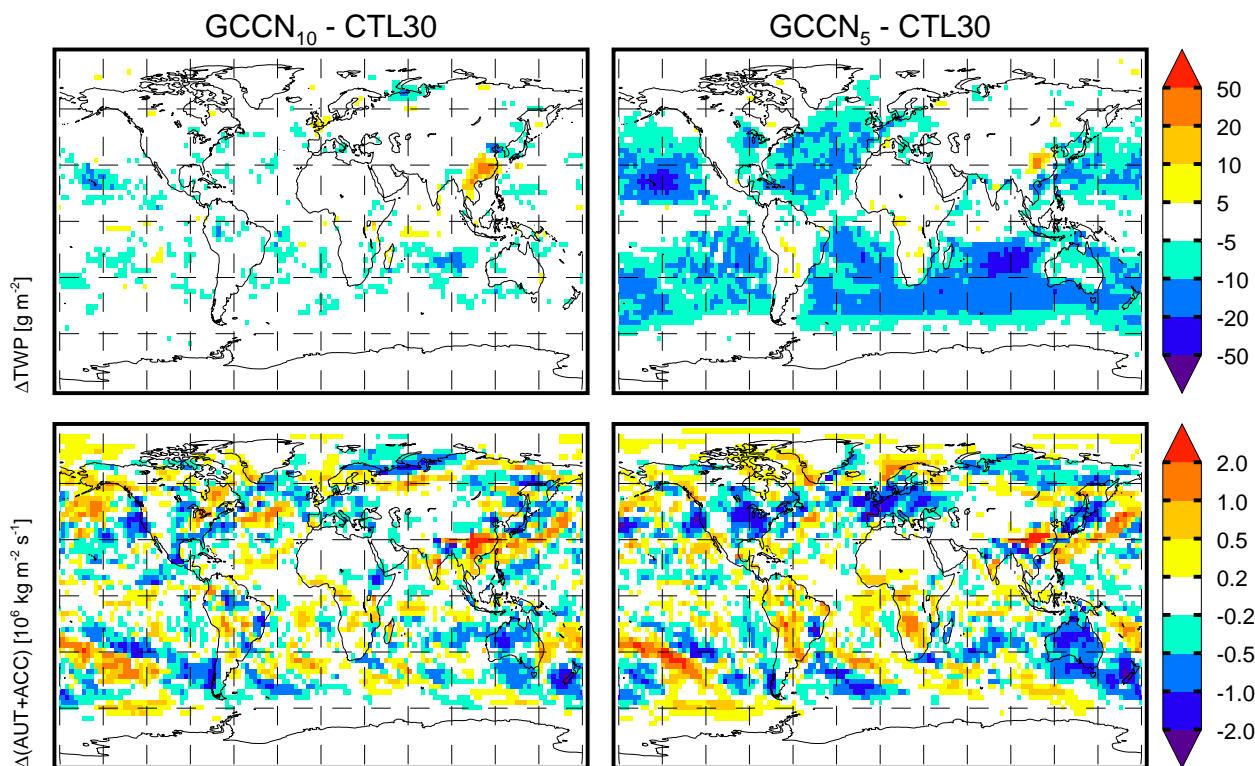


Fig. 9. Differences in the global distribution of TWP (upper row) and total conversion rate (autoconversion+accretion, lower row) between the GCCN₁₀ (left column) and GCCN₅ (right column) simulations and CTL30.

the large-scale moisture convergence which triggers convection and also determines whether the shallow or deep convection scheme is used. Thus, the patterns of convection are altered as shown in Fig. 10 (lower panel).

3.2.3 Present-day vs. Pre-industrial

The difference between present-day and pre-industrial simulations gives an estimate of the effect of anthropogenic aerosols on climate. Figure 11 shows the zonal mean changes of the GCCN concentration from pre-industrial to present-day climate. GCCN concentrations are closely linked to the 10 m wind speed (Fig. 12). Both simulations show an increase of wind speed in the southern storm tracks. But, GCCN₁₀ locates it more poleward than the GCCN₅-simulation. Towards the equator a band with decreasing wind speed follows. The wind speed in the northern hemisphere does not show a similar feature. Increasing wind speed lead to an increase of GCCN (and vice versa). Thus, the GCCN concentration increases especially over the southern hemisphere and to a smaller extend also over the northern hemisphere. Note that the GCCN concentrations for the GCCN₅-simulations are generally higher due to the smaller cutoff radius.

The total aerosol concentration is increasing vastly especially over the northern hemisphere. This increase is mainly attributed to human activity and industrial development. Hence, the GCCN ratio which is defined as the ratio between GCCN to total aerosol concentration is decreasing because the total aerosol increase is much larger than the increase in GCCN concentrations. Hence, the influence of the GCCN is larger in the present-day climate with high aerosol concentrations than it is in the pre-industrial climate as shown in the SCM sensitivity studies.

In Table 5 and Fig. 13 the differences in the annual global and zonal means due to anthropogenic aerosols for the ECHAM5 simulations are summarized, respectively. The changes in global precipitation due to anthropogenic activity are rather faint which is due to the application of fixed sea-surface temperatures within the simulations and, thus, fixed evaporation from the oceans no matter how many GCCN are present or how many sub-time steps are used in the prognostic rain scheme. The zonal mean differences for precipitation in Fig. 13 are rather noisy. Thus, the prognostic rain scheme and the incorporation of GCCN does not lead to systematic changes in the precipitation difference.

The anthropogenic changes in total global cloud cover (TCC) are also very small and have no clear tendency to more or less cloud cover with higher amounts of GCCN. Regions

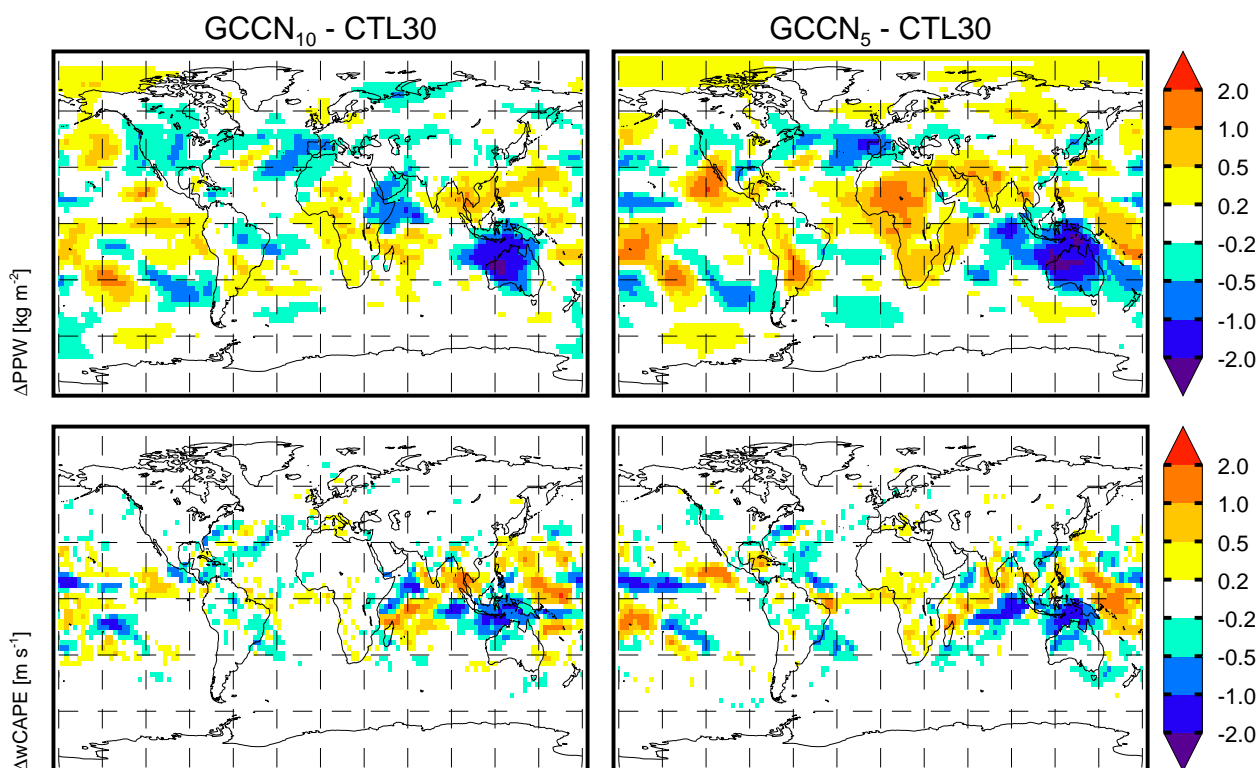


Fig. 10. Differences in the global distribution of PPW (upper row) and vertical velocity due to CAPE (lower row) between the GCCN₁₀ (left column) and GCCN₅ (right column) simulations and CTL30.

Table 5. Annual global mean changes and interannual standard deviations of cloud properties and TOA energy budget from PD to PI.

		CTL30		GCCN ₁₀		GCCN ₅		CTL10	
P_{tot}	[mm d ⁻¹]	0.001	±0.011	-0.001	±0.008	0.004	±0.007	0.001	±0.006
TCC	[%]	0.12	±0.18	0.18	±0.18	0.11	±0.14	0.12	±0.18
TWP	[g m ⁻²]	2.2	±0.74	2.1	±0.6	1.8	±0.51	2.4	±0.52
N_l	[10 ¹⁰ m ⁻²]	0.17	±0.4	0.19	±0.5	0.16	±0.3	0.19	±0.4
R_{eff}	[μm]	-0.16	±0.02	-0.16	±0.03	-0.17	±0.03	-0.14	±0.02
SW	[W m ⁻²]	-1.05	±0.24	-1.19	±0.31	-1.03	±0.23	-1.18	±0.26
LW	[W m ⁻²]	0.08	±0.14	0.15	±0.11	0.12	±0.22	0.12	±0.23
Net	[W m ⁻²]	-0.97	±0.19	-1.04	±0.29	-0.91	±0.27	-1.06	±0.35

with increased cloudiness due to the GCCN alternate with regions with decreased cloudiness in the zonal mean differences.

The incorporation of GCCN reduces the difference between present-day and pre-industrial TWP. Thus, the increase in TWP due to enhanced, anthropogenic aerosol numbers is partly compensated by the presence of GCCN. Cloud drop number and cloud drop effective radius are almost constant for all considered simulations and thus, do not show any significant tendency like the TWP in the global mean differences. The annual zonal mean differences give a more detailed insight into the anthropogenic changes of TWP and

cloud drop number and radius. The TWP and cloud drop number differences are largest in the northern hemisphere. Industrialization in Europe, North America and, recently, Asia result in enhanced aerosol number that act as CCN and influence cloud and precipitation formation. As Lohmann et al. (2007) stated the TWP increase is mainly due to a retardation of drizzle formation in clouds over the ocean. Hence, clouds (and cloud water) stay longer in the atmosphere. The presence of GCCN causes a reduction of the TWP and cloud drop number difference. Thus, the GCCN counteract the CCN increase and therefore reduce the aerosol indirect effects. Nevertheless, there are also regions (like the tropics,

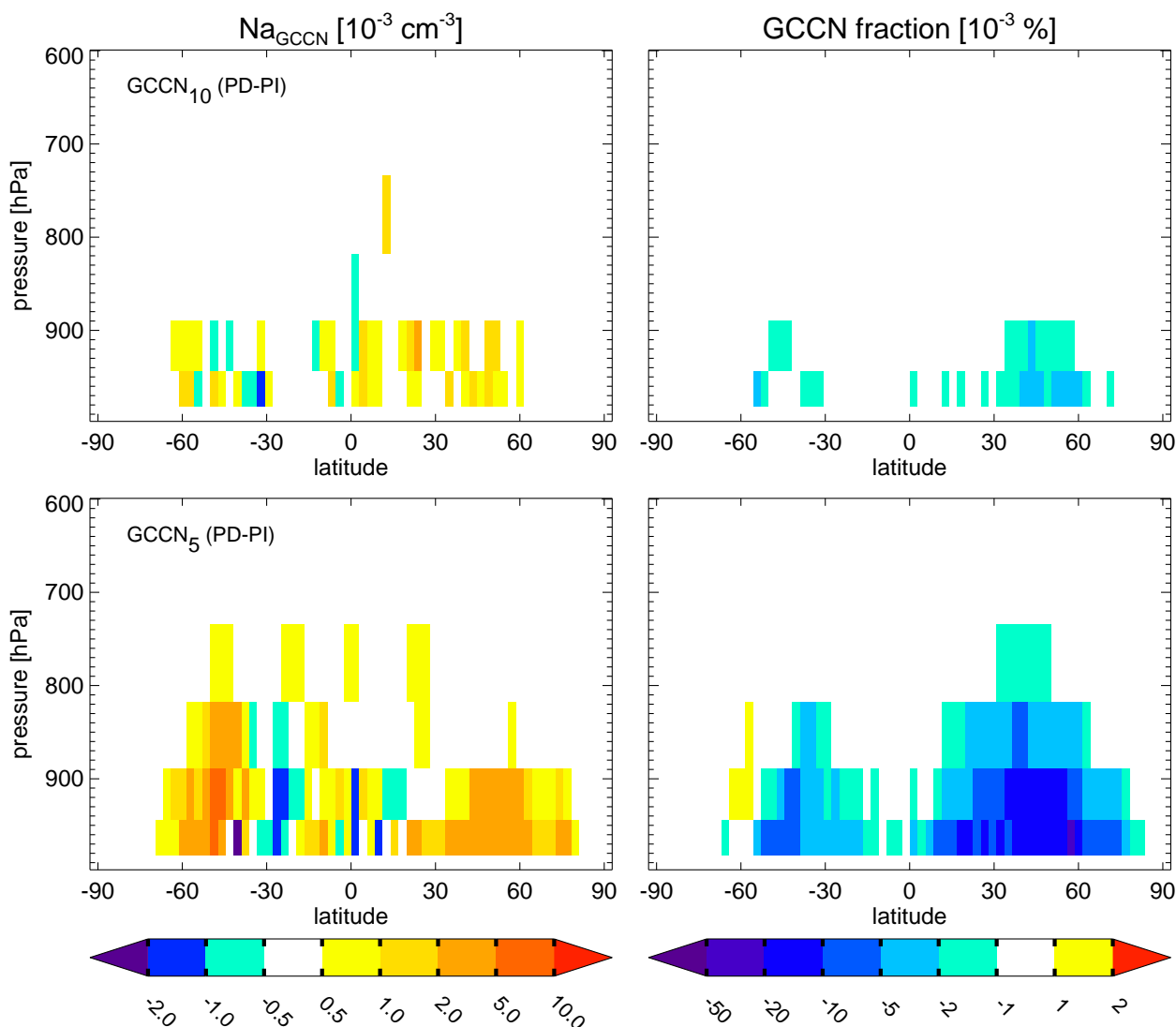


Fig. 11. Difference of zonal average of giant sea salt concentration and giant sea salt fraction between present-day and pre-industrial simulations of GCCN₁₀ (upper row) and GCCN₅ (lower row).

the subtropics and the high latitudes) where the incorporation of GCCN lead to an increase in TWP and N_1 from PI to PD. The changes of R_{eff} in the zonal means are only minor and are limited to the very high latitudes.

Closely connected to the cloud cover is the TOA radiative budget. The prognostic rain scheme lowers the effect of aerosols on the short-wave radiation. The obtained values of -1.05 Wm^{-2} for CTL30 and -1.18 Wm^{-2} for CTL10 are almost reduced by a factor of two compared to a value of -2.0 Wm^{-2} reported by Lohmann et al. (2007) for the standard ECHAM5. This is caused by the much smaller increase in TWP from PI to PD in these simulations. While TWP increased by 6.9 g m^{-2} from PI to PD in Lohmann et al. (2007), here the increase in TWP amounts to $1.8\text{--}2.4 \text{ g m}^{-2}$ in much better agreement to observations (e.g., Nakajima et al.,

2001). The incorporation of the GCCN does not lead to a further decrease of the short-wave radiation similar to the TCC. For the GCCN₁₀-simulation the short-wave radiation increases to -1.19 Wm^{-2} whereas for the GCCN₅-simulation the short-wave radiation decreases to -1.03 Wm^{-2} . The annual zonal mean differences show that the SW radiation difference is mainly increased in the northern midlatitudes because of the reduction of TWP in that region. Within the tropics and the higher latitudes the SW radiation is decreasing which is most likely due to changes in the convection patterns.

The long-wave (LW) radiation budget, which is closely connected to high clouds, shows much smaller differences between PI and PD. The prognostic rain scheme does not influence the long-wave radiation radiation very much. The

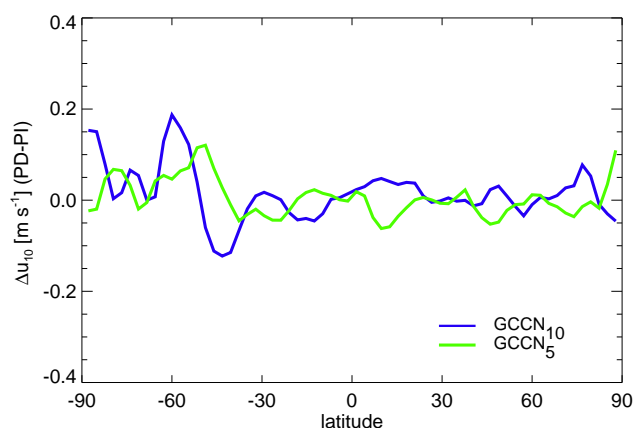


Fig. 12. Difference of 10m wind speed between present-day and pre-industrial simulations for GCCN₁₀ and GCCN₅.

obtained values of 0.08 Wm^{-2} for the CTL30 simulation and of 0.12 Wm^{-2} for the CTL10 simulation are similar to the value of 0.1 Wm^{-2} reported by Lohmann et al. (2007) for the standard ECHAM5. The incorporation of the GCCN does not change LW difference very much.

The difference in the net radiation between present-day and pre-industrial climate is referred to as the anthropogenic aerosol effect including the direct and indirect effects. The net radiative effect of anthropogenic aerosols is -0.97 Wm^{-2} for CTL30 and -1.06 Wm^{-2} for CTL10. Similar to the SW radiation, these values are almost a factor of two smaller than the net radiation value of -1.9 Wm^{-2} of the standard ECHAM5 (Lohmann et al., 2007). Incorporation of the GCCN do not have much influence on the net radiation budget and thus, on the aerosol indirect effect. For the GCCN₁₀-simulation the short-wave radiation increases to -1.04 Wm^{-2} whereas for the GCCN₅-simulation the short-wave radiation decreases to -0.91 Wm^{-2} . Again, no clear tendency of the net radiation with increasing amount of GCCN is given. However, the changes in the net radiation are small compared to the interannual variability. Thus, it can be concluded that the AIE hardly changes due to the incorporation of the GCCN. The discussion of the annual zonal means of the net radiation follows mainly the one for the SW radiation. Nevertheless, the changes in the long-wave radiation partly compensate the changes in the short-wave radiation.

For the present-day simulation it was found that the GCCN₅ and the CTL-simulation show similar results. Looking at the differences between PD and PI this cannot be found. CTL10 behaves much more like CTL30 than GCCN₅. The effect of GCCN is much stronger in PD climate as a higher number of CCN are present than in PI. Thus, for the GCCN₅-PD simulation the activation of GCCN into drizzle water cannot compensate anymore for the lower conversion rates. This causes a higher TWP for GCCN₅-PD and, consequently, a lower difference between PD and PI than for CTL10.

4 Conclusions

The effect of GCCN on the global climate, specifically on clouds and precipitation within a GCM, is investigated. The GCCN concentration is obtained by the tail of the (soluble/mixed) coarse mode distribution within the ECHAM5-HAM aerosol module for two different cutoff radii. GCCN are assumed to activate directly into rain drops because of their size. Within the model this is achieved by redistributing the total condensed water into cloud and rain water according to the number of GCCN and by assuming a rain drop size of $25 \mu\text{m}$.

Direct observations of GCCN are rare but measurements of sea salt size distributions are available for several locations over the globe. Integration of the measured distributions for sizes larger than the chosen cutoff radii of $5 \mu\text{m}$ and $10 \mu\text{m}$ gives GCCN concentrations that are compared to the GCCN concentration obtained by ECHAM5. The natural variability of the GCCN is not fully captured in the model because simulated sea salt emissions depend mainly on wind speed and not on other factors like relative humidity, stability, precipitation history and others. The GCCN concentration for the $10 \mu\text{m}$ cutoff agree much better with the measured concentrations. Furthermore, the concentrations are about ten times lower than for the $5 \mu\text{m}$ cutoff, which brings them in better agreement with the GCCN concentrations reported by Feingold et al. (1999). Globally, the GCCN are concentrated in the windy regions, namely the storm tracks of the northern and southern hemisphere. Less GCCN are found in calm regions like the tropics and along the west coasts of the continents.

Sensitivity studies with the SCM version of ECHAM5 are carried out with different GCCN and CCN concentrations as well as with different initial rain drop sizes in order to estimate the effect of GCCN on cloud microphysical quantities. The GCCN have an impact on the precipitation formation processes in the SCM and the used GCCN scheme is able to reproduce the results presented by Feingold et al. (1999). Nevertheless, larger GCCN concentrations are necessary in the SCM to obtain a noticeable effect. Too high GCCN concentrations assuming $55 \mu\text{m}$ rain drops lead to an exaggerated transfer of the condensed water to the rain class at the expense of the cloud water. In this case the autoconversion and accretion rates are reduced causing lower precipitation rates. This effect is an artifact in the model because in nature large drops grow slower than smaller drops and, thus, the rain drops would not grow to those large sizes because of kinetic limitations.

The introduction of the prognostic rain scheme into the ECHAM5-GCM leads to a strong decrease in the AIE compared to the standard ECHAM5-HAM GCM presented by Lohmann et al. (2007). This results mainly from a decreasing importance of the autoconversion in the rain formation process because it is the only microphysical (rain forming) process that depends on the cloud drop number and thus, on

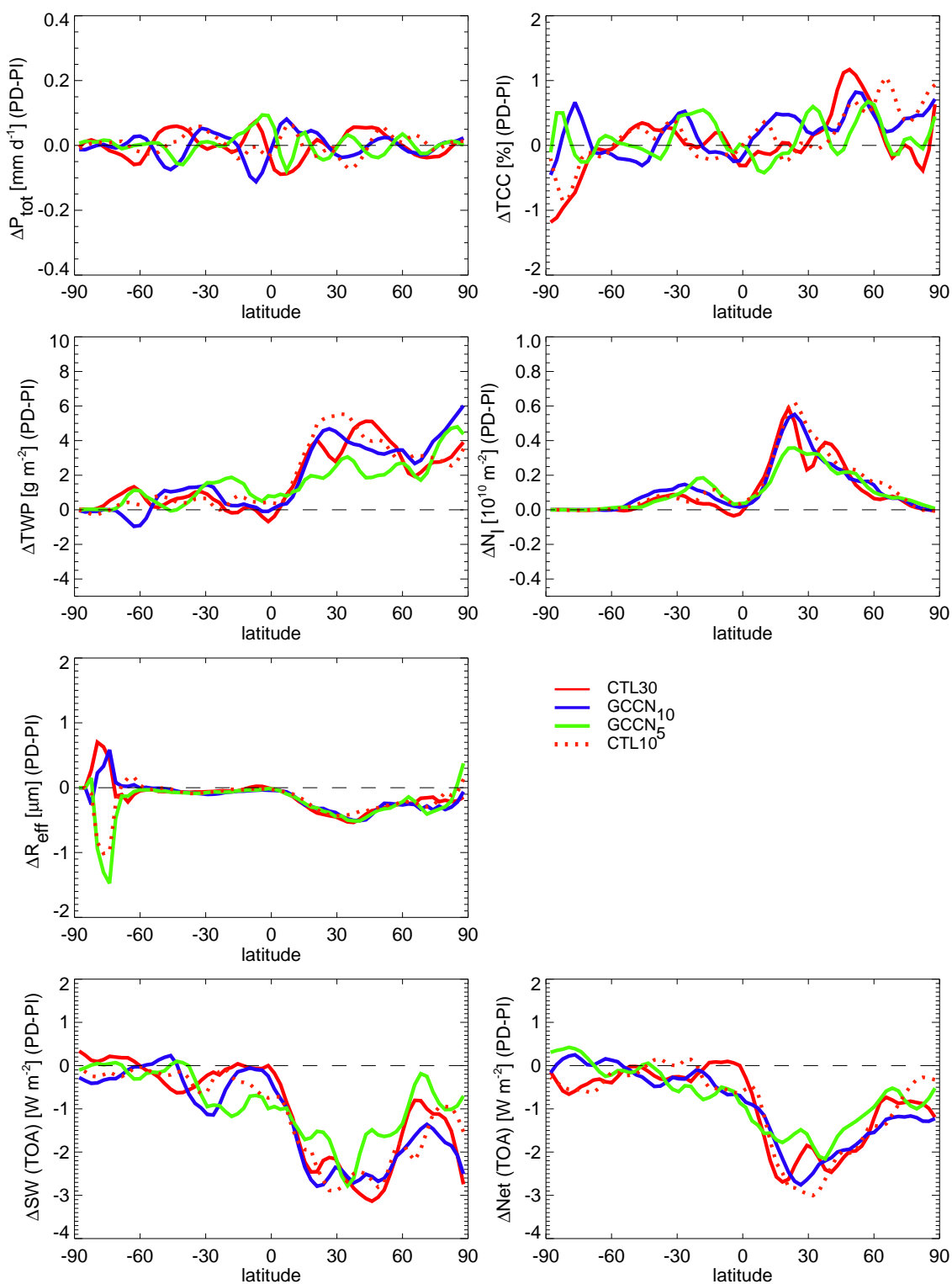


Fig. 13. Annual zonal means differences between the present-day and pre-industrial simulations of precipitation, total cloud cover, total water path, column integrated cloud droplet number, effective cloud droplet radius at cloud top ($T > 273.15\text{K}$) as well as short-wave and net radiation at TOA from CTL30, GCCN₁₀, GCCN₅, and CTL10 simulations.

the aerosol concentration, whereas, accretion depends only on the mass of cloud and rain water. The size on the AIE does hardly depend on the number of sub-time steps within the prognostic rain scheme for the shown simulations with 30 and 10 sub-time steps. Further differences due to the number of sub-time steps arise only for in-cloud properties like TWP, N_1 and R_{eff} which are also directly affected by the changes in the conversion rates. This leads also to changes in cloud cover and consequently the short-wave cloud forcing. Other variables like precipitation, and long-wave cloud forcing do not show any dependence on the sub-time step number.

The incorporation of the GCCN in the ECHAM5-GCM results in rather faint changes in the precipitation. In the global and zonal averages hardly any differences are detectable. The global patterns are zonally redistributed meaning that regions with an increasing precipitation rates alternate with regions with decreasing precipitation rates so that the zonal average does not change. Interestingly, the rather small changes in the large-scale precipitation patterns feed back to the convective precipitation scheme due to changes in the global moisture field. The subsequent changes in the convective precipitation rates are larger than the changes in the large-scale precipitation rates.

Nevertheless, the GCCN change cloud properties such as TWP and N_1 regionally and globally. This is mainly due to the transfer of condensed water to rain water and only to a very small part to the changes in the conversion rates. For the simulations with the $10\ \mu\text{m}$ cutoff the changes are rather small because small GCCN concentration result in a low transfer of water to the rain phase. The GCCN₅-simulation show a ten times higher GCCN burden and, thus, more rain water is gained by the activation of GCCN. This results in a stronger decrease of the TWP. The enhanced transfer in this case is able to compensate for the decrease in the total conversion rates.

The main differences between present-day and pre-industrial simulations with the ECHAM5-GCM are found for TWP and N_1 in the midlatitudes of the northern hemisphere where the strongest increase in anthropogenic aerosols is observed. The changes in cloud properties lead to subsequent changes in the radiative budget of the earth. Zonal means show that the SW budget becomes less negative in the regions where TWP and N_1 decrease. The same is true for the net radiation budget, but changes in the LW budget partly compensate changes in the SW-budget. In those regions, GCCN are able to counteract the effects of increased aerosol loads in the present-day climate. In the tropics the incorporation of the GCCN leads to the opposite effect so that the net radiation budget becomes more negative. In the annual global mean this leads to a nearly constant net radiation difference between PD and PI. Thus, on a global scale the GCCN do not influence the radiation budget and therefore do not compensate for the effects of increased aerosol loads in PD.

Nevertheless, it is likely that improvements to the ECHAM5-GCCN simulations might change the presented

results. This improvements will include a more sophisticated numerical treatment of the sedimentation of rain drops in the prognostic rain scheme. The treatment of the GCCN activation should be treated separately to include the competition for the available water vapor during condensational growth and to account for the preferred activation of larger CCN. Furthermore, the condensational growth of the GCCN and CCN shall be done explicitly to avoid the application of the very rigid rain drop formation radius of $25\ \mu\text{m}$ and to avoid unphysically high transfer ratios that might appear for quite high GCCN concentrations.

Acknowledgements. The authors thank P. Spichtinger and D. Cziczo (ETH Zurich) and two anonymous reviewers for helpful comments and suggestions, P. Stier (Univ. of Oxford) and S. Ferrachat (ETH Zurich) for their support with the ECHAM5-HAM and the Swiss National Supercomputing Centre (CSCS) for computation time.

Edite by: K. Carslaw

References

- Adler, R. F., Huffman, G. J., Chang, A., Ferraro, R., Xie, P. P., Janowiak, J., Rudolf, B., Schneider, U., Curtis, S., Bolvin, D., Gruber, A., Susskind, J., Arkin, P., and Nelkin, E.: The version-2 Global Precipitation Climatology Project (GPCP) monthly precipitation analysis (1979-present), *J. Hydrometeorol.*, 4, 1147–1167, 2003.
- Albrecht, B. A.: Aerosols, cloud microphysics, and fractional cloudiness, *Science*, 245, 1227–1230, 1989.
- Andreas, E. L.: A new sea spray generation function for wind speeds up to $32\ \text{m s}^{-1}$, *J. Phys. Oceanogr.*, 28, 2175–2184, 1998.
- Andreas, E. L., Monahan, E. C., Rouault, M. P., and Smith, S. D.: The spray contribution to net evaporation from the sea – A review of recent progress, *Bound.-Lay. Meteorol.*, 72, 3–52, 1995.
- Beheng, K. D. and Doms, G.: A general formulation of collection rates of cloud and raindrops using the kinetic equation and comparison with parameterizations, *Beitr. Phys. Atmosph.*, 59, 66–84, 1986.
- Bretherton, C. S., Uttal, T., Fairall, C. W., Yuter, S. E., Weller, R. A., Baumgardner, D., Comstock, K., Wood, R., and Raga, G. B.: The EPIC 2001 stratocumulus study, *Bull. Amer. Meteorol. Soc.*, 85, 967–977, 2004.
- Cooper, W. A., Bruintjes, R. T., and Mather, G. K.: Calculations pertaining to hygroscopic seeding with flares, *J. Appl. Meteorol.*, 36, 1449–1469, 1997.
- Denman, K. L., Brasseur, G., Chidthaisong, A., Ciais, P., Cox, P. M., Dickinson, R. E., Hauglustaine, D., Heinze, C., Holland, E., Jacob, D., Lohmann, U., Ramachandran, S., da Silva Dias, P. L., Wofsy, S. C., and Zhang, X.: Couplings Between Changes in the Climate System Biogeochemistry, in: *Climate Change 2007: The Physical Science Basis. Contribution of Working Group I to the Fourth Assessment Report of the Intergovernmental Panel on Climate Change*, edited by Solomon, S., Qin, D., Manning, M., Chen, Z., Marquis, M., Averyt, K., M. Tignor, and Miller, H., chap. 7, 499–588, Cambridge University Press, Cambridge, United Kingdom and New York, NY, USA, 2007.

- Dentener, F., Kinne, S., Bond, T., Boucher, O., Cofala, J., Generoso, S., Ginoux, P., Gong, S., Hoelzemann, J. J., Ito, A., Marelli, L., Penner, J. E., Putaud, J. P., Textor, C., Schulz, M., van der Werf, G. R., and Wilson, J.: Emissions of primary aerosol and precursor gases in the years 2000 and 1750 prescribed data-sets for AeroCom, *Atmos. Chem. Phys.*, 6, 4321–4344, 2006, <http://www.atmos-chem-phys.net/6/4321/2006/>.
- Feingold, G., Cotton, W. R., Kreidenweis, S. M., and Davis, J. T.: The impact of giant cloud condensation nuclei on drizzle formation in stratocumulus: Implications for cloud radiative properties, *J. Atmos. Sci.*, 56, 4100–4117, 1999.
- Fitzgerald, J. W.: Marine aerosols - A Review, *Atmos. Environ.*, 25, 533–545, 1991.
- Ghate, V. P., Albrecht, B. A., Kollias, P., Jonsson, H. H., and Breed, D. W.: Cloud seeding as a technique for studying aerosol-cloud interactions in marine stratocumulus, *Geophys. Res. Lett.*, 34, L14807, doi:10.1029/2007GL029748, 2007.
- Greenwald, T. J., Stephens, G. L., Vonderhaar, T. H., and Jackson, D. L.: A physical retrieval of cloud liquid water over the global oceans using Special Sensor Microwave Imager (SSM/I) observations, *J. Geophys. Res.-Atmos.*, 98, 18 471–18 488, 1993.
- Guelle, W., Schulz, M., Balkanski, Y., and Dentener, F.: Influence of the source formulation on modeling the atmospheric global distribution of sea salt aerosol, *J. Geophys. Res.-Atmos.*, 106, 27 509–27 524, 2001.
- Hahn, C. J., Warren, S. G., and London, J.: Climatological data for clouds over the globe from surface observations, 1982-1991: The total cloud edition, Tech. rep., ORNL/CDIAC-72 NDP-026A Oak Ridge National Laboratory, Oak Ridge Tennessee, USA, 1994.
- Han, Q. Y., Rossow, W. B., and Lacis, A. A.: Near-global survey of effective droplet radii in liquid water clouds using ISCCP data, *J. Clim.*, 7, 465–497, 1994.
- Han, Q. Y., Rossow, W. B., Chou, J., and Welch, R. M.: Global variation of column droplet concentration in low-level clouds, *Geophys. Res. Lett.*, 25, 1419–1422, 1998.
- Huffman, G. J., Adler, R. F., Arkin, P., Chang, A., Ferraro, R., Gruber, A., Janowiak, J., McNab, A., Rudolf, B., and Schneider, U.: The Global Precipitation Climatology Project (GPCP) Combined Precipitation Dataset, *Bull. Amer. Meteorol. Soc.*, 78, 5–20, 1997.
- Johnson, D. B.: The Role of Giant and Ultragiant Aerosol Particles in Warm Rain Initiation, *J. Atmos. Sci.*, 39, 448–460, 1982.
- Khairoutdinov, M. and Kogan, Y.: A New Cloud Physics Parameterization in a Large-Eddy Simulation Model of Marine Stratocumulus, *Mon. Weather Rev.*, 128, 229–243, 2000.
- Kiehl, J. T., Hack, J. J., and Briegleb, B. P.: The simulated earth radiation budget of the national Center for Atmospheric Research Community Climate Model CCM2 and comparisons with the Earth Radiation Budget Experiment (ERBE), *J. Geophys. Res.-Atmos.*, 99, 20 815–20 827, 1994.
- Levin, Z., Teller, A., Ganor, E., and Yin, Y.: On the interactions of mineral dust, sea-salt particles, and clouds: A measurement and modeling study from the Mediterranean Israeli Dust Experiment campaign, *J. Geophys. Res.-Atmos.*, 110, D20202, doi:10.1029/2005JD005810, 2005.
- Lewis, E. R. and Schwartz, S. E.: Sea Salt Aerosol Production - Mechanisms, Methods, Measurements, and Models, vol. 152 of *Geophysical Monograph*, American Geophysical Union, 2004.
- Lin, H. and Leaitch, R.: Development of an In-Cloud Aerosol Activation Parameterization for Climate Modelling, in: WMO Workshop on Measurements of Cloud Properties for Forecasts of Weather and Climate, Mexico City, June 1997, 1997.
- Lohmann, U. and Diehl, K.: Sensitivity studies of the importance of dust ice nuclei for the indirect aerosol effect on stratiform mixed-phase clouds, *J. Atmos. Sci.*, 63, 968–982, 2006.
- Lohmann, U. and Roeckner, E.: Design and performance of a new cloud microphysics scheme developed for the ECHAM general circulation model, *Clim. Dynam.*, 12, 557–572, 1996.
- Lohmann, U., Stier, P., Hoose, C., Ferrachat, S., Kloster, S., Roeckner, E., and Zhang, J.: Cloud microphysics and aerosol indirect effects in the global climate model ECHAM5-HAM, *Atmos. Chem. Phys.*, 7, 3425–3446, 2007, <http://www.atmos-chem-phys.net/7/3425/2007/>.
- Monahan, E. C., Spiel, D. E., and Davidson, K. L.: Oceanic whitecaps and their role in air-sea exchange, chap. A model of marine aerosol generation via whitecaps and wave disruption, pp. 167 – 174, D. Reidel, Norwel, Mass., 1986.
- Nakajima, T., Higurashi, A., Kawamoto, K., and Penner, J. E.: A possible correlation between satellite-derived cloud and aerosol microphysical parameters, *Geophys. Res. Lett.*, 28, 1171–1174, 2001.
- Nordeng, T. E.: Extended versions of the convective parameterization scheme at ECMWF and their impact on the mean and transient activity of the model in the tropics, Technical Memorandum 206, ECMWF, Reading, UK, 1994.
- O'Dowd, C. D., Smith, M. H., Consterdine, I. E., and Lowe, J. A.: Marine aerosol, sea-salt, and the marine sulphur cycle: A short review, *Atmos. Environ.*, 31, 73–80, 1997.
- Posselt, R. and Lohmann, U.: Introduction of prognostic rain in ECHAM5: Design and Single Column Model simulations, *Atmos. Chem. Phys. Discuss.*, 7, 14 675–14 706, 2007.
- Reid, J. S., Jonsson, H. H., Smith, M. H., and Smirnov, A.: Evolution of the vertical profile and flux of large sea-salt particles in a coastal zone, *J. Geophys. Res.-Atmos.*, 106, 12 039–12 053, 2001.
- Roeckner, E., Bäuml, G., Bonaventura, L., Brokopf, R., Esch, M., Giorgetta, M., Hagemann, S., Kirchner, I., Kornblueh, L., Manzini, E., Rhodin, A., Schlese, U., Schulzweida, U., and Tompkins: The atmospheric general circulation model ECHAM5, Part I: Model description, Tech. Rep. 349, Max-Planck-Institute for Meteorology, Hamburg, Germany, 2003.
- Rosenfeld, D., Lahav, R., Khain, A., and Pinsky, M.: The role of sea spray in cleansing air pollution over ocean via cloud processes, *Science*, 297, 1667–1670, 2002.
- Rossow, W. B. and Schiffer, R. A.: Advances in understanding clouds from ISCCP, *Bull. Amer. Meteorol. Soc.*, 80, 2261–2287, 1999.
- Rotstayn, L. D.: A physically based scheme for the treatment of stratiform clouds and precipitation in large-scale models (1): Description and evaluation of the microphysical processes, *Q. J. R. Meteor. Soc.*, 123, 1227–1282, 1997.
- Schulz, M., de Leeuw, G., and Balkanski, Y.: Emissions of atmospheric trace compounds, chap. Sea-salt aerosol source functions and emissions, 333–359, Kluwer Academic Publishers, 2004.
- Seifert, A. and Beheng, K. D.: A double-moment parameterization for simulating autoconversion, accretion and selfcollection, *Atmos. Res.*, 59, 265–281, doi:doi:10.1016/S0169-8095(01

- 00126-0, 2001.
- Smith, M. H. and Harrison, N. M.: The sea spray generation function, *J. Atmos. Sci.*, 29, 189–190, 1998.
- Smith, M. H., Consterdine, I. E., and Park, P. M.: Atmospheric loading of marine aerosol during a hebridean cyclone, *Q. J. R. Meteor. Soc.*, 115, 383–395, 1989.
- Stier, P., Feichter, J., Kinne, S., Kloster, S., Vignati, E., Wilson, J., Ganzeveld, L., Tegen, I., Werner, M., Balkanski, Y., Schulz, M., and Boucher, O.: The aerosol-climate model ECHAM5-HAM, *Atmos. Chem. Phys.*, 5, 1125–1156, 2005, <http://www.atmos-chem-phys.net/5/1125/2005/>.
- Sundqvist, H., Berge, E., and Kristjansson, J. E.: Condensation and cloud parameterization studies with a mesoscale numerical weather prediction model, *Mon. Weather Rev.*, 117, 1641–1657, 1989.
- Susskind, J., Piraino, P., Rokke, L., Iredell, T., and Mehta, A.: Characteristics of the TOVS Pathfinder Path A dataset, *Bull. Amer. Meteorol. Soc.*, 78, 1449–1472, 1997.
- Tegen, I., Harrison, S. P., Kohfeld, K., Prentice, I. C., Coe, M., and Heimann, M.: Impact of vegetation and preferential source areas on global dust aerosol: Results from a model study, *J. Geophys. Res.-Atmos.*, 107, 4576, 2002.
- Tiedtke, M.: A comprehensive mass flux scheme for cumulus parameterization in large-scale models, *Mon. Weather Rev.*, 117, 1779–1800, 1989.
- Twomey, S.: Pollution and planetary albedo, *Atmos. Environ.*, 8, 1251–1256, 1974.
- Weng, F. Z. and Grody, N. C.: Retrieval of cloud liquid water using the Special Sensor Microwave Imager (SSM/I), *J. Geophys. Res.-Atmos.*, 99, 25 535–25 551, 1994.
- Wentz, F. J.: A well-calibrated ocean algorithm for SSM/I, *J. Geophys. Res.-Oceans*, 102, 8703–8718, 1997.
- Wood, R.: Drizzle in stratiform boundary layer clouds. Part II: Microphysical aspects, *J. Atmos. Sci.*, 62, 3034–3050, 2005.
- Woodcock, A. H.: Salt nuclei in marine air as a function of altitude and wind force, *J. Meteorol.*, 10, 362–371, 1953.
- Zhang, L. M., Michelangeli, D. V., and Taylor, P. A.: Influence of aerosol concentration on precipitation formation in low-level, warm stratiform clouds, *J. Aerosol. Sci.*, 37, 203–217, 2006.